Title

Microanatomical changes and biomolecular expression at the PDL-entheses during experimental tooth movement

Journal

Journal of Periodontal Research, 54(3)

ISSN

0022-3484

Authors

Yang, Lynn
Kang, Misun
He, Rui
et al.

Publication Date

2019-06-01

DOI

10.1111/jre.12625

Peer reviewed

HHS Public Access

Author manuscript

J Periodontal Res. Author manuscript; available in PMC 2020 June 01.

Published in final edited form as:

J Periodontal Res. 2019 June ; 54(3): 251–258. doi:10.1111/jre.12625.

Micro-anatomical changes and biomolecular expression at the PDL-entheses during experimental tooth-movement

L. Yang[1], **M. Kang**[1], **R. He**[1], **B. Meng**[2], **MR. Arvin Pal**[1], **L. Chen**[1], **A.H. Jheon**[2], and **S.P. Ho**[1,*]

[1]Division of Biomaterials and Bioengineering, Department of Preventive and Restorative Dental Sciences, School of Dentistry, University of California San Francisco, CA 94143

[2]Division of Craniofacial Anomalies, Department of Orofacial Sciences, School of Dentistry, University of California San Francisco, CA 94143

Abstract

The novel aspect of this study is to contextualize the co-localization of biomolecular expression in widened and narrowed periodontal ligament (PDL) space within a mechanically activated periodontal complex. The PDL is unique as it is the only ligament with both innervation and vascularization. Maxillary molars in 6-week old male C57BL/6 mice (N=5) were experimentally translated for two weeks using an elastic spacer. Contralateral teeth were used as controls. Mechanical testing of the periodontal complex of a mouse *in situ* and imaging using an X-ray micro-computed tomography (micro-XCT) illustrated deformations within blood vessels (BV) of the PDL under load. PDL-bone and PDL-cementum entheses at the widened and narrowed PDL-spaces following experimental tooth movement (ETM) illustrated osterix (OSX), bone sialoprotein (BSP), cluster of differentiation 146 (CD146), and protein gene product 9.5 (PGP9.5), indicating active remodeling at these sites. PGP9.5 positive nerve bundles (NBs) were co-localized with multinucleated cells (MCs), Howship's resorption lacunae, and CD146 positive BVs. Association between nerves and MC was complemented by visualizing the proximity of osmium tetroxide stained NBs with the ultrastructure of MCs by performing scanning transmission electron microscopy. Spatial association of NB with BV, and NB with MC, provided insights into the plausible co-activation of NBs to initiate osteoclastic activity. Resorption of mineral occurs as an attempt to restore PDL-space of the load bearing complex, specifically at the PDL-entheses. Mapping of anatomy-specific structural elements and their association with regenerative molecules by correlating light and electron micrographs can provide insights into the use of these extracellular matrix molecules as plausible targets for pharmacological interventions related to tooth movement. Within the realm of tissue regeneration, modulation of load can reverse naturally occurring mineral formation to experimentally-induced resorption, and naturally occurring mineral resorption to experimentally-induced formation at the enthesial sites in order to permit tooth translation.

[*]Corresponding author: Sunita P. Ho, Ph.D., Division of Biomaterials and Bioengineering, Department of Preventive and Restorative Dental Sciences, 513 Parnassus Avenue, HSW813, University of California San Francisco, San Francisco, CA 94143, sunita.ho@ucsf.edu.

1. INTRODUCTION

Full-fixed orthodontic appliances supply active forces to teeth that naturally drift mesially in humans. In mice and rats, passive forces on the dentoalveolar complex facilitate natural *distal* drift[1]. The rate of natural mesial drift is maintained by chewing[2] and altered by forces from orthodontic appliances. It is critical to acknowledge that orthodontic forces and moments will either augment or counteract these passive forces. Conceivably, moving teeth in the direction of or opposite to natural drift could lead to reversal of hard tissue resorption and formation. The intended manipulation of biological processes from resorption to formation, and formation to resorption, create experimental tooth movement (ETM).

In the load-bearing dentoalveolar complex, resorption of bone, cementum, and even dentin are inevitable, resulting in a significantly translated tooth. Moving the hard structure such as a tooth-root relative to another hard structure, the alveolar bone with a limited PDL-space of 70μm (150μm to 400μm in humans[4]) necessitates tissue remodeling and thereby significant changes in bone and cementum[5]. “Sculpting” of bone and cementum is an attempt to maintain homogenous PDL-space through a crosstalk between mechanically activated blastic and clastic biological events. In the PDL, mechanoreceptors (Ruffini-like endings) and nociceptors are wrapped around blood vessels (BVs)[6], and these neurovascular bundles are expected to be co-localized. Interestingly, in the pain-inducing clinical intervention of orthodontics, there is limited knowledge on spatiotemporal distribution and density of neurovasculature in addressing the regenerative potential of this unique PDL and the maintenance of attachment of a softer ligament to a harder mineralized tissue. As a first step toward the overall goal, the objective of this study is to understand the localization of matrix molecules at targeted regions of the spatially-altered dentoalveolar complex resulting from a mechanical stimulus on the tooth-crown. The specific aim of this study is to correlate micro-anatomical biological responses within the dentoalveolar complex on two-dimensional (2D) histological sections with physical perturbations in three-dimensional (3D) PDL-spaces resulting from forces on the tooth-crown. What is the effect of the net force on the 3D PDL-space? Do orthodontists consider adjusting the magnitude of orthodontic force if moving teeth with or against the direction of natural drift? More specifically to this manuscript and within the realm of the aforementioned questions, under these mechanical manipulations, does the neurovascular density at the micro-anatomical locations of the PDL-bone and PDL-cementum entheses shift toward the direction in which the force is applied? This study will provide insights into the latter question by correlating widened and narrowed regions in the 3D PDL-space with immunolocalized mechanosensitive matrix proteins, increased innervation at the PDL-bone entheses juxtaposed with increased vascular density, and osteogenic markers during ETM.

2. MATERIALS AND METHODS

2.1. *In vivo* model for ETM

An ETM study on C57BL/6 male mice (N = 5) at six weeks of age was conducted in compliance with the guidelines of the Institutional Animal Care and Use Committee of UCSF, protocol number AN148450–01B using Waldo method and as described previously[7]. After 14 days, the hemi-maxillae were fixed overnight in 10% neutral buffered formalin

(Richard-Allan Scientific, Kalamazoo, MI) and stored in 70% ethanol aqueous solution at 4°C.

2.2. X-ray micro computed tomography (Micro-XCT) and post-analyses of CT data sets

Each specimen was scanned using an X-ray micro computed tomography (Micro-XCT 200, Carl Zeiss, Pleasanton, CA) at 2X magnification. After digital reconstruction, the 3D data were further processed by AVIZO® software (9.0.1, FEI, Hillsboro, Oregon) to extract the direction of torque, displacement of molars, 3D movements of molars relative to each other, and displacement relative to the alveolar socket in control and experimental groups resulting from ETM as described in the appendix. Torque results from ETM when the force (vector) resulting from the elastic spacer acts away from the center of mass of the tooth; eccentric load[8]. Altered PDL-space for the first molar over time is demonstrated by registering images from control groups with those from experimental groups. The normalized frequency of PDL-space for each specimen was plotted for control and experimental groups. There were two experimental groups, and the contralateral hemimaxillae served as controls. T=0 included mice sacrificed immediately after tooth-movement was initiated. T=2 included mice sacrificed after 2 weeks of tooth-movement.

2.3. *In situ* imaging of a mechanically loaded PDL

Physical perturbations to PDL-space were determined by first visualizing the complex under loaded conditions using an *in situ* imaging technique[8]. Control specimens (N = 3) of C57BL/6 mice at age 8 weeks were immediately euthanized, dissected, then immersed in phosphotungstic acid for an hour to enhance X-ray contrast of PDL at no load and under 7 Newtons (N) of load, and imaging parameters were similar to that mentioned before. The digital data was analyzed using AVIZO® software and as described in the appendix.

2.4. Scanning transmission electron microscopy (STEM) of osmicated periodontal complex

A first molar (M1) and the adjoining PDL and alveolar bone was sectioned from the left hemi-maxilla of an 8-week C57BL/6 mouse, and fixed overnight in 10% neutral buffered formalin (Richard-Allan Scientific, Kalamazoo, MI). The specimen was then washed three times for 20 minutes each in 1X PBS, and stored in 70% ethanol aqueous solution at 4°C. To perfuse the specimen with OsO4, it was placed in 4 ml of 1% OsO4 for 3 hours, then rinsed 5 times for 15 minutes each in 0.1 M sodium cacodylate buffer and transferred to 50% ethanol. The osmicated specimen was then embedded and ultrasectioned to 90 nm of thickness placed on a formvar/carbon-coated Ni grid (Electron Microscopy Sciences) grid and was visualized using STEM (Sigma 500 aSTEM detector, Carl Zeiss Microscopy, Pleasanton, CA).

2.5. Histology and immunolocalization of matrix proteins in the periodontal complex

Following Micro-XCT scanning, the specimens were decalcified for 2 weeks using 0.5 M EDTA (pH=8.0) solution, and were processed for paraffin sectioning with a microtome (Microm HM 325, ThermoScientific, Fremont, CA) into 5–6 μm transverse sections. Following deparaffinization, sections were stained with hematoxylin and eosin (H&E)) and

serial sections were used for immunolocalization of biomolecules of interest. Epitope retrieval on serial sections was achieved with 0.1 M sodium citrate buffer (pH=6.0) for 30 minutes at 80°C. The matrix proteins bone sialoprotein (BSP), osterix (OSX), cluster of differentiation (CD146) and protein gene product (PGP9.5) were colocalized in tissue sections (seeappendix) and examined at 40X using a light microscope (Zeiss Observer Z1, Axiocam 506).

2.6. Correlative light and electron microscopy (CLEM) on histology sections

Following imaging under a light microscope, the coverslip of each histology slide was removed and the slides were dehydrated using graded (50–100%) ethanol solutions and visualized by scanning electron microscopy (SEM) (Sigma 500, Carl Zeiss Microscopy, Pleasanton, CA). Immunolocalized regions were correlated with ultrastructures of the matrix by aligned distinct tissue characteristics observed in both light and electron micrographs.

3. RESULTS

3.1. Movement of teeth relative to each other and to the alveolar socket

Following image registration of experimental and control hemi-maxillae, the movement of molars in the control group at T=0 (Figs.1:IA, IB, IC) and ETM group (Figs.1:IID, IIE, IIF) are shown by the highlighted centers of rotation and arrows displaying the angle of torque. Registered and segmented molars (M1, M2, M3) are overlaid to display global tooth movement for both groups (Fig.1:IB & IIE). Tooth displacement frequency graphs demonstrate the relative displacement trends of each group (Fig.1:IC & IIF). The movement of teeth as depicted by the vectors for M2 and M3 (Fig.1:IA & IID) were significantly altered at time T=2 weeks compared to that observed at T=0 weeks. By comparing T=0 weeks with T=2 weeks, it is evident that M2 and M3 were significantly translated and rotated at both time points (Figure 1:IA and IID). However, this trend did not hold true for M1. M1 movement at T=2 weeks was significantly greater than that at T=0 as seen by the longer vector (white arrows). PDL-space was analyzed (Fig.2:IA & IIC) to demonstrate the changes in PDL-space with elastic dam placement. The shift in PDL-space is depicted with a color map (Fig.2:IB & IID). These alterations in PDL-space for the molars over time (T=0 and T=2weeks) are shown in Figs.2IIIE & 2IIIF, where T=2 EXP is shown to have distinctly higher frequency of widened PDL-space values (Supplemental Fig. 2).

3.2. Colocalization of matrix proteins in altered PDL-spaces

PDL-space is color-mapped on the surface of M1 roots with three transverse sections of the T=2weeks ETM group (Fig.3A). The values of the PDL-space surrounding the three roots (R1, R2, R3) of the transverse section in the middle (red rectangular area, Fig.3A) is depicted as a separate virtual 2D section (Fig.3B). White rectangles correspond to the widened zone (WZ) and narrowed zone (NZ) (Fig.3B) of R2. Immunohistochemistry on serial sections (Fig.3C) show CD146 in high concentrations in both the WZ and NZ with overall higher prevalence in WZs. PGP9.5 appeared in higher concentrations associated with BVs at the PDL-alveolar bone entheses and multi-nucleated cells in Howship's lacunae. BSP localization was higher in the widened zone near the PDL-alveolar bone entheses,

compared to the areas with multinucleated cells in the compression zone, while OSX was at a higher intensity near PDL-alveolar bone entheses and around BVs.

3.3. Correlative maps of neurovascular bundles and multi-nucleated cells

Overlaying the light micrographs and scanning electron micrographs (Figs.4g & 4h), imaged from a PGP9.5 immunolocalized histological section of T=2 week ETM (Fig.3C) resulted in a CLEM image (Figure 4f) indicating clear co-localization of the PGP9.5 neuronal marker with the multinucleated cells in Howship's lacunae (HL) resorption pits and juxtaposed with BVs (Fig.4f, red arrows). Scanning transmission electron micrographs (Figs.4i, 4j, 4k) illustrated the same pattern of a MC adjacent to the HL with nearby NBs.

3.4. Visualization of deformed blood vessels within a loaded periodontal complex

Data from micro-XCT *in situ* mechanical testing of a dentoalveolar complex (Fig.4a) illustrated the change in periodontal space as indicated by narrowed and widened regions (scale bar) (Fig.4b), as well as clear deformation of BVs within the compressed complex (Figs.4c and 4d, white arrows).

4. DISCUSSION

Mechanobiological processes involved in "sculpting" of bone and cementum to maintain PDL-space under eccentric loading underscore the effects of mechanical strain not limited to the PDL, but also at the PDL-entheses, which illustrate the "plastic" nature of the dentoalveolar complex. Orthodontic tooth movement exceeds physiologic PDL-space, deforms the PDL, and prompts local inflammation. The specific goal of this study was to correlate expressions of osteogenic matrix markers, neuronal cell bodies and/or axons, and endothelial cells within the narrowed and widened regions of the innervated and vascularized PDL in the 3D-complex during ETM.

The spatial location of biochemical expressions in 2D histology sections as seen using a light microscope were correlated in 3D-space as seen using reconstructed volumes from X-ray scans. In the X-ray scans, definitive regions indicated by narrowed and widened PDL-spaces can be observed with ETM at T=0, and this trend was also observed in specimens at T=2weeks of elastic dam placement. Based on the histograms, interestingly, the peak values of experimental specimens were similar to that of the control at T=0 and T=2weeks, although the frequency at which these values were observed were significantly lower for control compared to experimental group (Figs.2, A and C, frequency between control and experimental curves at T=0 and T=2weeks). However, with 2 weeks of containing the elastic spacer between M1 and M2, it is likely that the initially narrowed region specifically of R1M1 at time T=0 became narrower in various quadrants of the complex of M1, and that this expression is highlighted through varying levels of tissue remodeling such as mineralization (Fig.3, rectangles in Supplemental Fig.3). Interestingly, in the same M1, an effect of overall increased PDL-space was observed at the distal-half of M1R2, and was recorded predominantly as bone resorption with presence of osteoclastic activity and HL (Fig.4). We postulate that the compression mediated mineralization and tension-mediated resorption can result from a rapid application of force on a tooth-crown resulting in an

osteoclastic response rather than conventionally believed tension-mediated osteoblastic activity.

During ETM, narrowed zones indicate compression of tissues and would undergo bone and cementum resorption. This implies that narrowed PDL-space should be correlated with increased localization of osteoclastic cells for resorption, which in this study were observed in widened regions. Additionally, observed increased mineralization (Supplemental Fig.3, red arrows) in the narrowed region of M1 contradicts the notion of bone resorption. These contradicting patterns underscore the importance of correlating histological observations with physical perturbations in a 3D-space to investigate the causality of force on the tooth-crown. In this study, the osteogenic potential of PDL is also highlighted, albeit being a consequence of significantly stronger compression. The ability of the PDL to promote mineral formation and resorption for some same mode of force that is noticeably compression, but likely of different magnitude and rate, brings credence to its regenerative potential. Additionally, when deformations within the PDL need to be finely tuned during orthodontic therapy, it is necessary to control resorption and/or formation within the periodontal complex with the understanding that all that is widened need not illicit tension based biological process and vice versa. However, the effect of a “Goldilocks” scenario must be considered; what is an optimum magnitude of force that should be delivered, and how can an orthodontist gauge force to maintain a functional dentoalveolar joint? These questions are minimally investigated as most studies have assumed a qualitative approach on physical perturbations.

From a mechanics of materials perspective, the load transmitting sites of PDL-cementum and PDL-bone entheses are postulated to undergo strain-amplification regardless of physiologic or non-physiologic loads on the tooth-crown. Additionally, at these sites several hypertrophic progenitors positive for OSX, a bone progenitor marker, were observed. It is conceivable that mineral formation, which is identified through increased expressions of BSP[9] are expressed at the PDL-bone entheses (Fig.3C). The osteoid-like less mineralized layer at the PDL-bone entheses also contains BVs. Based on CLEM, BVs are juxtaposed with nerves and are spatially in close proximity to the PDL-bone entheses. Under loaded (physiologic or pathologic) conditions, various constituents that define the complex undergo deformation, including the vasculature and nerves which make the ligament of the complex under mechanical load unique compared to the musculoskeletal ligaments. Specifically, at the PDL-bone enthesial zone, the expression of precursor CD146 related to endothelial intercellular junction remodeling of blood vessels was co-localized with the expression of PGP9.5, indicating appositional PDL nerve involvement with blood vessels at the mechanosensitive sites of the loaded complex (Figure 4, Supplemental Figure 4). It is postulated that this specific localization of BVs and nerves are to govern mineral formation- and resorption-related biological events as a function of shifts in mechanical strains through neurogenic inflammation. By immunolocalization of PGP9.5[11] and CD146[12], we observed nerves and vasculature juxtaposed at both the blastic and clastic zones (Fig.3C). The CLEM image allowed us to confirm the structural association of BVs with DAB-stained areas of PGP9.5, as both are juxtaposed with HL (Figs.4f, 4g, 4h, and Supplemental Fig.4). STEM micrographs of osmium tetroxide stained nerve bundles in close proximity to a multi-nucleated cell adjacent to HL further reflected the association of nerves with osteoclastic

activity (Figs.4i, 4j, 4k, Supplemental Fig.5). This association has been demonstrated to be critical for the regulation of osteoclastic activity through transection studies[13]. As such, it is conceivable that biomolecular distribution shifts in the PDL-space during ETM reflect amplified biological responses of passive tooth drift. We propose that the demonstrated presence of multi-nucleated cells, nerve bundles and blood vessels at Howship's lacunae at a widened zone after two weeks of ETM is a consequence of previously compressed narrowed PDL-space undergoing remodeling to re-establish physiologic PDL-space.

The effect of acute and chronic inflammatory cascades can persist at the PDL-bone and PDL-cementum enthesial zones. Prolonged sterile inflammation as a result of ETM requires a biomolecular network; however, biomolecular expressions vary with magnitude and duration of forces. Specimens at multiple time points would allow for analyses of protein expressions over time, and as such our T=2 weeks experimental results are not necessarily indicative of the dynamic process that the complex undergoes. The initial forces exerted by the spacers cannot be directly comparable to altered effect of forces over time of the experimental groups as the complex remodels.

In general, the two phases of ETM are acute inflammation and then rapid recovery and reconstruction of the PDL[14] to sustain load-mediated demands. The inflammatory stage requires transportation of cytokines, blood cells, and gas exchange[15]; these biological demands may necessitate angiogenesis. Angiogenesis as a result of ETM is facilitated by the signaling through mechanosensitive elements, such as the nerves in the PDL, which are postulated to increase their expression during inflammation. Nociceptor sensitivity to cytokines from immune cell signaling and the subsequent release of neuropeptides may lead to further immune cell activation. The deformation of the blood vessels under mechanical loading (Figs.4a, 4b, 4c, 4d, and Supplemental Fig.1) suggests hypoxia due to vasoconstriction. Our experimental results demonstrated an increase in CD146 in the PDL surrounding M1 relative to controls. This observation supports the idea of an increase in angiogenesis arising over the course of ETM in contrast to the expression during natural tooth drift (Fig.3C). The relatively lower vascular density in tissue sections from control specimens, provided insights into the possible roles of angiogenesis in response to ETM (Fig. 3). Nerves as stained by PGP 9.5 appear to be closely associated with the CD146 stained blood vessels (Fig.4), and suggest their shared role in the inflammatory response towards ETM. With mechanosensitive and noxious pain receptors, stimulated sensory neurons are able to signal and influence the progression of inflammatory responses, and as such affect blood flow and capillary network action, all of which can challenge the biomechanical characteristics of the dynamic PDL.

5. CONCLUSIONS

Mechanical strains from the spacer augmented naturally programmed biological processes. Bimolecular events resulting in distal resorption and mesial formation could be dependent on the "sudden shifts" in physical perturbations. Data provides insights into the need to "recalibrate", in that the current dogma that compression results in resorption, and that tension results in formation, is load rate sensitive. Depending on the distribution of stress over the periodontal complex, the rate-related effects of mechanobiological strains can be

spread through quadrants, thirds, or halves of the complex, and need not be uniformly spread over the root length (Figs.2, Supplemental Fig.2). By targeting only the mesial and distal regions within a rodent model in 2D plane, seminal information in other locations may be overlooked. Additional novel insights into plausible sensory nerve activation through increased expression and co-localization of PGP9.5 with CD146 positive BVs indicated their co-activation in regions containing resorption pits denoted by osteoclasts. We postulate a potential "activation" of sensory nerves and vascular conduction that could initiate osteoclastic activity, where osteoclasts from hematopoietic origin act as agents that attempt to re-establish physiologic PDL-space. Within the same micrographs, the narrowed complex can be OSX positive and mineralize over time, and contradicts the argument that compression leads to hypoxia, nerve activation, and clastic events. Results provide insights into the strain-mediated biomolecular events, and reinforce the concept that these events are also sensitive to rate (fast or slow) of mechanical strains. Whether this synergistic clastic and blastic effects works toward maintaining sustained optimum function will continue to remain a question until the excursion of load-mediated stress from the tooth-crown to the individual tissues and their interfaces are correlated with site-specific biological outcomes both in space and time. This study is a first step toward the overall objective; multiscale mapping of mechanistic process by linking physical perturbations to biological outcomes that would allow for identification of key molecules for regeneration. Regeneration of soft and hard tissue entheses is identified through reactionary outcomes, which can be related to a "tug of war" between resorption and formation events, resulting in tooth translation. An inevitable pathologic function can arise unless forces on tooth-crowns, mechanical strains in the PDL and PDL-entheses, and resulting biological outcomes are calibrated to maintain optimum biomechanical function of the dentoalveolar fibrous joint.

Supplementary Material

Refer to Web version on PubMed Central for supplementary material.

ACKNOWLEDGEMENTS

Support was provided by NIH/NIDCR R01DE022032 (SPH), NIH/NIDCR R21DE027138 (SPH), NIH-NIDCR/R00DE022059 (AJ) and Departments of Preventive and Restorative Dental Sciences, and Orofacial Sciences, School of Dentistry, UCSF. The authors thank Biomaterials and Bioengineering Correlative Microscopy Core (BBCMC) at UCSF for their facilities and use of MicroXCT-200 and Sigma500 FESEM.

REFERENCES

1. Belting CM, Schour I, Weinmann JP, Shepro MJ. Age changes in the periodontal tissues of the rat molar. J Dent Res 1953; 32(3): 332–353. [PubMed: 13061672]
2. Sved A The mesial drift of teeth during growth. Am J Orthod 1955; 41(7): 539–553.
3. Feller L, Khammissa RAG, Thomadakis G, Fourie J, Lemmer J. Apical external root resorption and repair in orthodontic tooth movement: Biological events. BioMed Res Int 2016; 2016: 1–7.
4. Cate T, Nanci A. Ten Cate's - Oral Histology: Development, Structure, and Function. 8th Ed. 2012 St. Louis, MO: Elsevier.
5. Pal A, Chen L, Yang L, Yang F, Meng B, Jheon A, Ho SP. Micro-anatomical responses in the periodontal complex to calibrated orthodontic forces on the crown. *Orthod Craniofac* Res 2017; 20(S1): 100–105. [PubMed: 28643923]

6. Krishnan V Z Davidovitch. On a path to unfolding the biological mechanisms of orthodontic tooth movement. J Dent Res 2009; 88(7): 597–608. [PubMed: 19641146]

7. Waldo CM, Rothblatt JM. Histologic Response to Tooth Movement in the Laboratory Rat. J Dent Res 1954; 33(4): 481–486. [PubMed: 13184036]

8. Jang AT, Lin JD, Seo Y, Etchin S, Merkle A, Fahey K, Ho SP. In situ Compressive Loading and Correlative Noninvasive Imaging of the Bone-periodontal Ligament-tooth Fibrous Joint. J Vis Exp 2014; (85): 196–207.

9. Baht GS, Hunter GK, Goldberg HA. Bone sialoprotein-collagen interaction promotes hydroxyapatite nucleation. Matrix Biol 2008; 27(7): 600–8. [PubMed: 18620053]

10. Lindhe J, Lang NP, Karring T. Clinical Periodontology and Implant Dentistry, 5th Edition 2009 Oxford, UK: John Wiley & Sons.

11. Wilson PO, Barber PC, Hamid QA, Power BF, Dhillon AP, Rode J, Day IN, Thompson RJ, Polak JM. The immunolocalization of protein gene product 9.5 using rabbit polyclonal and mouse monoclonal antibodies. Br J Exp Pathol 1988; 69(1): 91–104. [PubMed: 2964855]

12. Bardin N, Francès V, Lesaule G, Horschowski N, George F, Sampol J. Identification of the S-Endo 1 Endothelial-Associated Antigen. Biochem Biophys Res Commun 1996; 218(1): 210–216. [PubMed: 8573133]

13. Yamashiro T, Fujiyama K, Fujiyoshi Y, Inaguma N, Takano-Yamamoto T. Inferior alveolar nerve transection inhibits increase in osteoclast appearance during experimental tooth movement. Bone 2000; 26(6): 663–9. [PubMed: 10831939]

14. Tsuge A, Noda K, Nakamura Y. Early Tissue Reaction in the Tension Zone of PDL during Orthodontic Tooth Movement. Arch Oral Biol 2016 65: 17–25. [PubMed: 26828679]

15. Masella RS, Meister M. Current Concepts in the Biology of Orthodontic Tooth Movement. Am J Orthod Dentofacial Orthop 2006; 129(4): 458–468. [PubMed: 16627170]

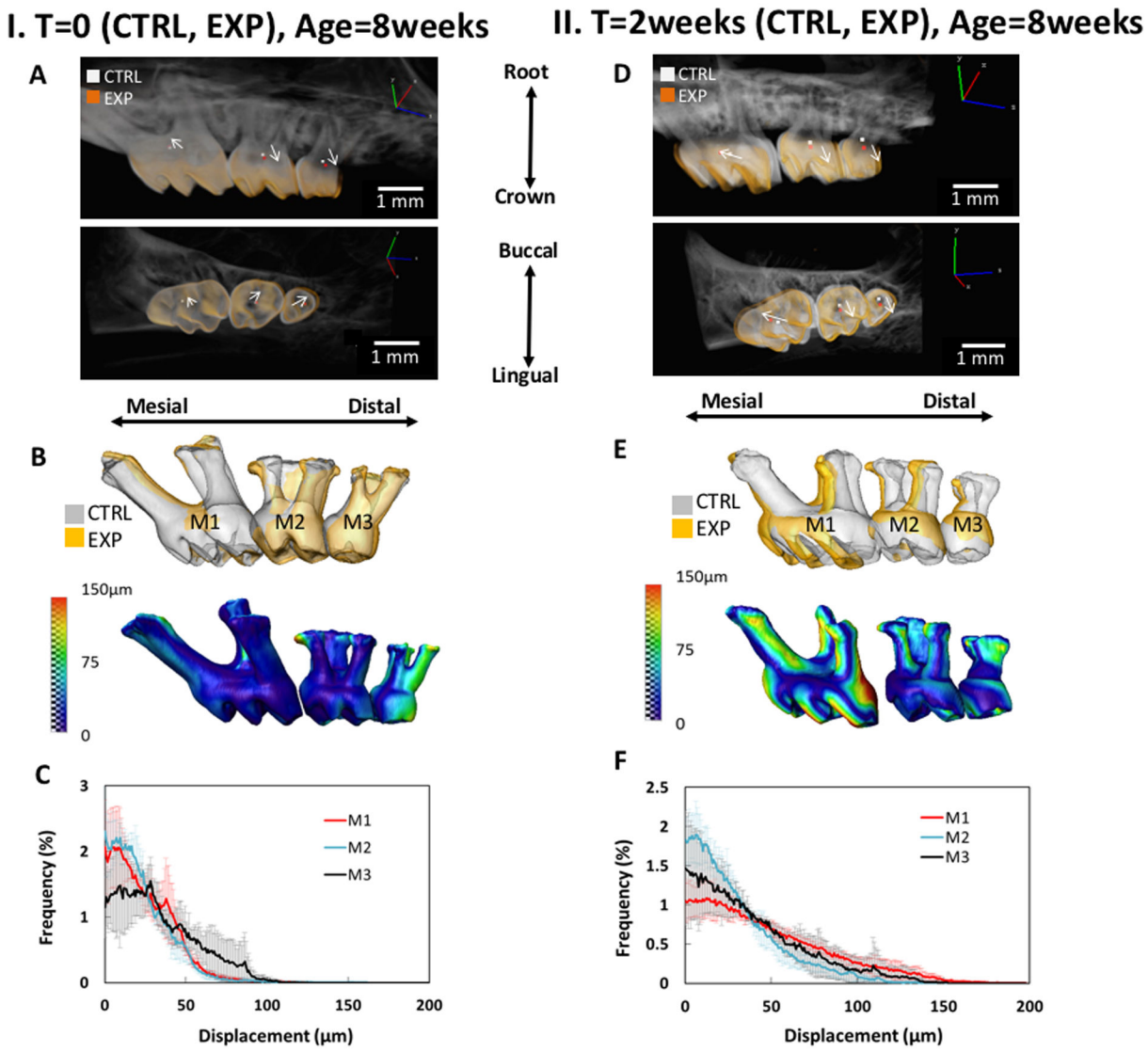

Figure 1. Temporal tooth movement and rotation:

Global tooth movement and rotation of molars M1-M3 following experimental tooth movement (ETM) after T=0 (IA, IB, IC) and T=2weeks (IID, IIE, IIF) of dam placement. Experimental and contra-lateral control hemi-maxillae were overlaid and registered (IA)&(IID), with the centers of rotation of each tooth highlighted in white (control - CTRL) and orange (experimental - EXP) (see left hand corner legend in IA and IID). Arrows connect the centers of rotation of the CTRL and EXP, displaying the angle of torque (IA) & (IID). Global tooth movement of M1-M3 are shown as a color map on tooth-root surfaces (IB)&(IIE). Displacement frequency graphs demonstrate relative tooth displacement trends for T=0 and T=2 weeks (IC)&(IIF).

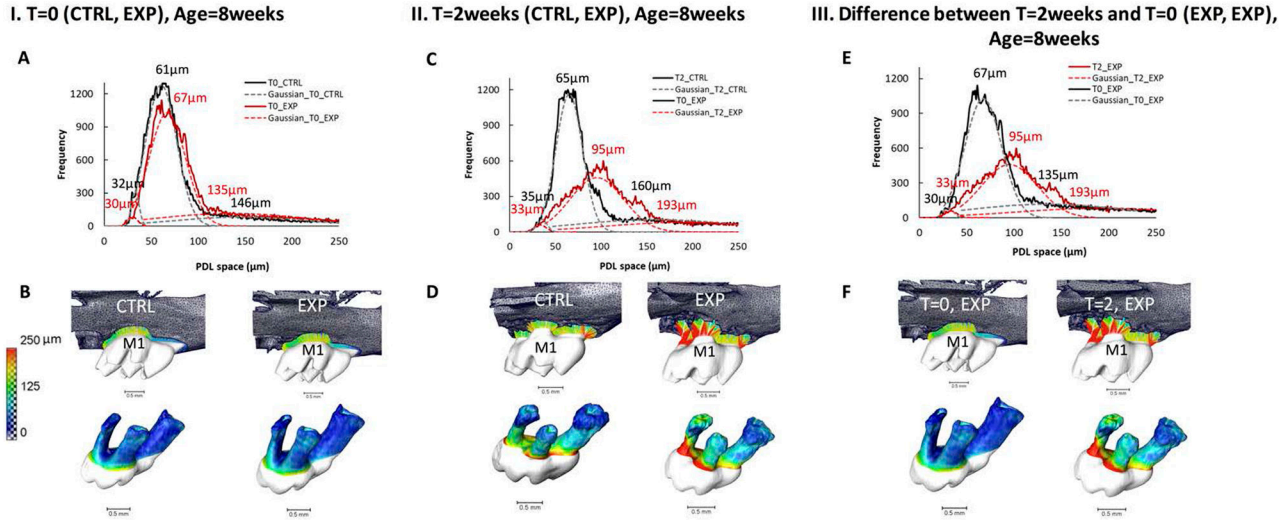

Figure 2. Changes in PDL-space over time:

PDL-space of the first molar subjected to experimental tooth movement (ETM) for T=0 in a representative 8 week old mouse (IA, IB), and for T=2 (2 weeks of placement of elastic dam in 6 week old mouse, and euthanized at 8 weeks of age) (IIC, IID) are shown as a color map on tooth-root surfaces. A Gaussian fit is applied to the graphed PDL-spaces and significant peaks were labeled (IA, IIC). The PDL-space is color-mapped (IB, IID). Gaussian-fit curves and graphed PDL-spaces are overlaid for experimental sides of the first molar for both T=0 and T=2 (IIIE). Differences in PDL-space of experimental sides of the first molar for both T=0 and T=2 weeks are shown by side by side color maps on the tooth-root surface (IIIF). See Supplemental Figure 2 for details on average PDL-space changes.

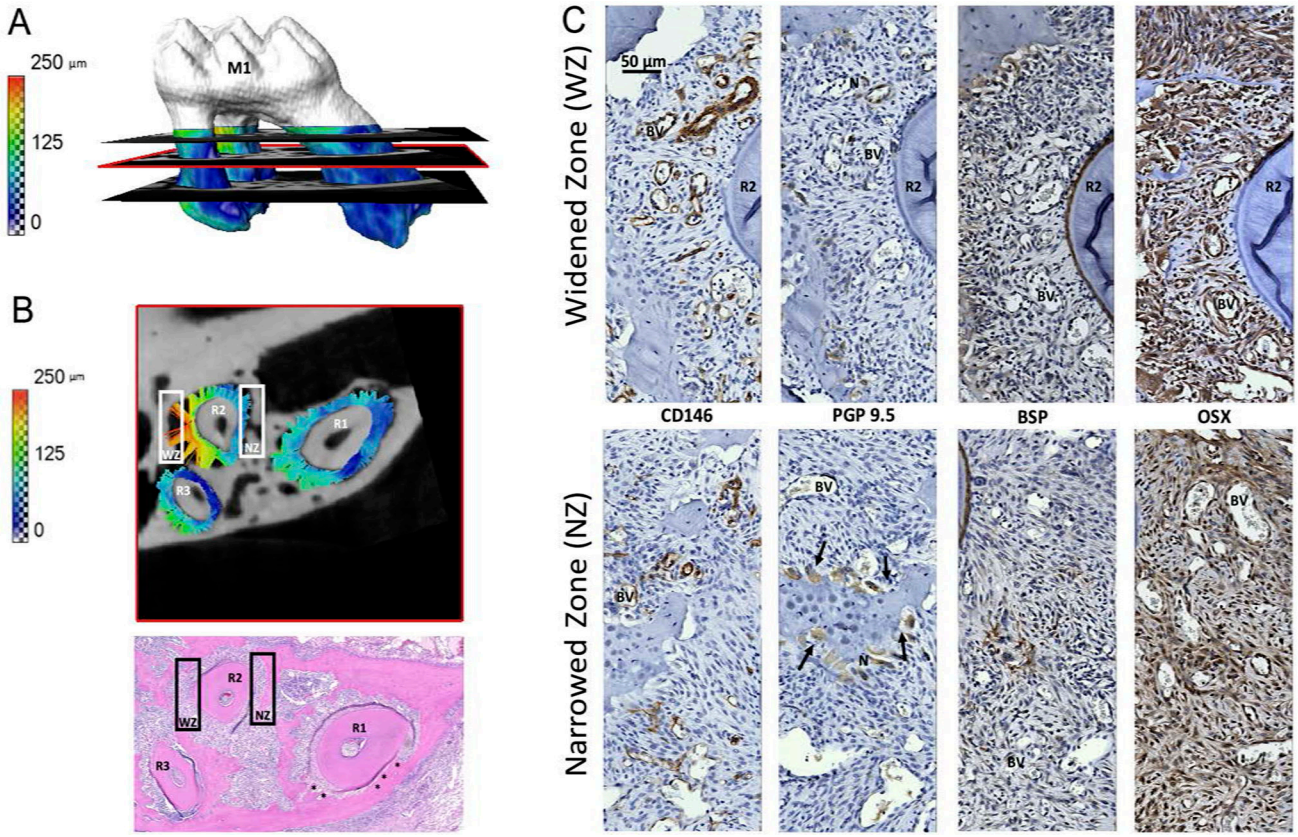

Figure 3. Correlating anatomical location with site-specific biological expressions within the periodontal complex:

(A) PDL-space after 2 weeks of experimental tooth movement (ETM) is color-mapped on the surfaces of the root of first maxillary molar (M1). A transverse virtual section containing change in PDL-space for roots one, two and three (R1, R2, R3) as indicated by colored tethers (pseudo ligament) is shown in detail in (B). A corresponding H&E stained transverse section, with bony growths indicated by asterisks, is shown for histological reference. The anatomy-specific immunolocalization of proteins (C) is from locations within the white rectangles in (B). White rectangles correspond to narrowed and widened zone (NZ, WZ). (C) Immunohistochemistry on serial transverse sections illustrate (left to right) cluster of differentiation 146 (CD146), protein gene product 9.5 (PGP), bone sialoprotein (BSP), osterix (OSX). Top row shows protein expressions within corresponding WZ, and bottom row shows the corresponding NZ results. BV: blood vessel, N: nerves, R1: first root, PDL: periodontal ligament, OB, OC, AB. All images were taken at 40X magnification and displayed at the same scale (top left image scale bar is 50 μm).

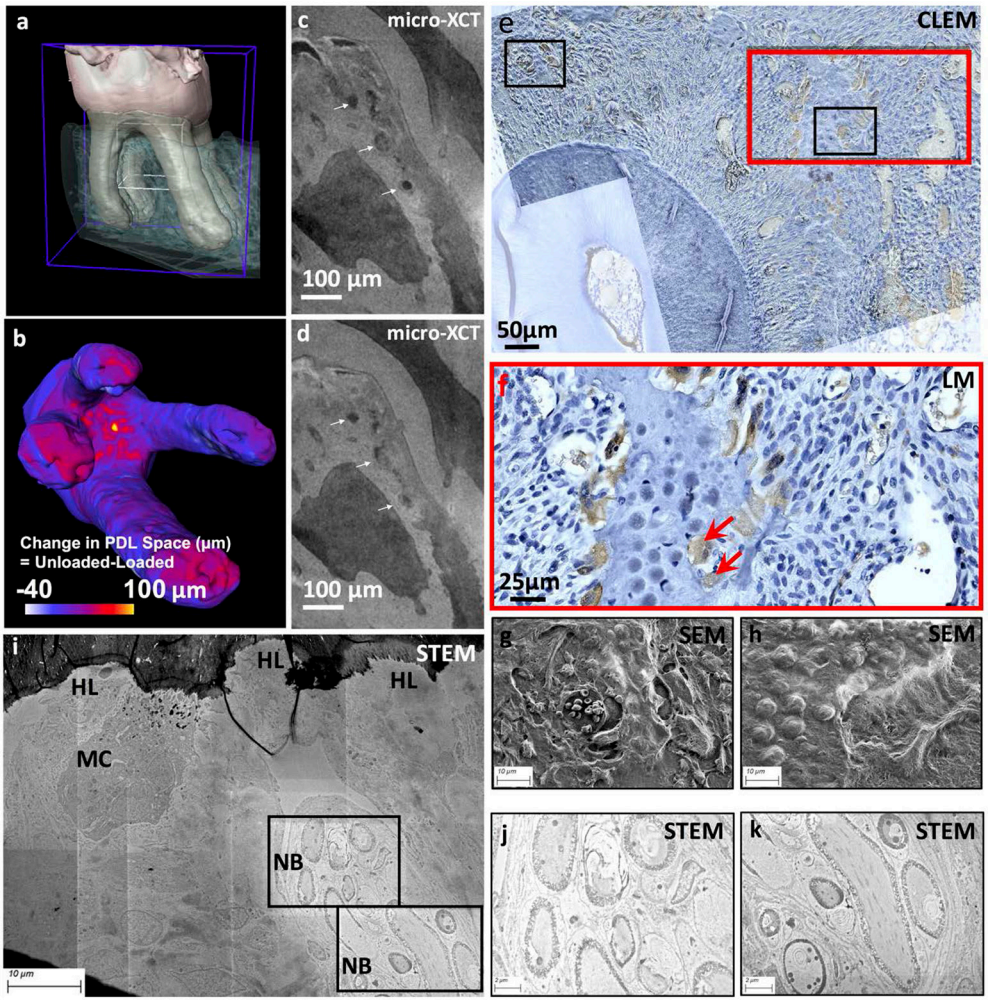

Figure 4. Visualization of blood vessels within a loaded periodontal complex, and the association of blood vessels with nerves and cells:

The dentoalveolar complex is shown in (a), and under load, the change in periodontal space as indicated by narrowed (−ve) and widened (+ve) regions (scale bar) is shown in (b). Data from micro-XCT illustrated deformed blood vessel (BV) within a loaded periodontal complex (white arrows, c, d). **Multiscale mapping and co-localization of blood vessels, nerves and multi-nucleated cells:** CLEM image (e) illustrates localization of PGP9.5 (brown stain) within the periodontal complex containing resorption pits (Howship's lacunae, HL) and multinucleated cells (f, MC, red arrows). Spatial association of nerves with blood vessels is shown in (g) and (h) SEM micrographs. At a higher resolution using STEM technique, osmium tetroxide stained nerve bundles (NB) in association with multinucleated cell (MC) including the ultrastructure of NB is shown in (j) and (k). Note: **CLEM: Correlative Light and Electron Microscopy, SEM: Scanning Election Microscopy, STEM: Scanning Transmission Election Microscopy**